Journal of Power Sources 214 (2012) 337–343

Contents lists available at SciVerse ScienceDirect

Journal of Power Sources

journal homepage: www.elsevier.com/locate/jpowsour

Ethanol reforming using $Ba_{0.5}Sr_{0.5}Cu_{0.2}Fe_{0.8}O_{3-\delta}$/Ag composites as oxygen transport membranes

C.Y. Park [a,*], T.H. Lee [a], S.E. Dorris [a], J.-H. Park [b], U. Balachandran [a]

[a] Energy Systems Division, Argonne National Laboratory, Argonne, Illinois 60439, USA
[b] Materials Science Division, Argonne National Laboratory, Argonne, Illinois 60439, USA

HIGHLIGHTS

- Cobalt-free OTMs, BSCF and its composites, BSCF/10–40 vol.% Ag, were fabricated.
- The oxygen permeation flux of the composites was measured.
- An Rh catalyst-coated composite was tested for producing H_2 from EtOH reforming.
- The composite with catalyst shifted EtOH conversion toward production of H_2.
- The Rh catalyst also increased the selectivity for H_2 and decreased coke formation.

ARTICLE INFO

Article history:
Received 2 March 2012
Received in revised form
20 April 2012
Accepted 21 April 2012
Available online 28 April 2012

Keywords:
Composite
Oxygen transport membrane (OTM)
Hydrogen production
Thermal expansion coefficient (TEC)
Ethanol reforming
Rh catalyst

ABSTRACT

Cobalt-free oxygen transport membranes (OTMs), $Ba_{0.5}Sr_{0.5}Cu_{0.2}Fe_{0.8}O_{3-\delta}$ (BSCF) and its composites, $Ba_{0.5}Sr_{0.5}Cu_{0.2}Fe_{0.8}O_{3-\delta}$/Ag (BSCF/Ag), were fabricated by conventional solid state synthesis, and their oxygen transport properties were evaluated. The metal (Ag) content in the composite was 10–40 vol.%. Based on oxygen-permeation results, BSCF/40 vol.% Ag with Rh catalyst was selected for testing its ability to supply high-purity oxygen (from air) for ethanol reforming. It was found that the composite played an important role in producing hydrogen from ethanol reforming at 600 °C. The composite with catalyst shifted ethanol conversion toward production of hydrogen and away from production of other products, i.e., using a catalyst increased the selectivity for hydrogen in the reformate. The crystal structure, thermal expansion, coke formation, and the microstructural behavior of the OTMs are discussed.

1. Introduction

Development of membrane materials for producing hydrogen as an alternative fuel is desirable due to the limited supply of fossil fuels. Oxygen transport membranes (OTMs) are of interest because of their diverse applications: the separation of oxygen from air [1–4], the conversion of natural gas to syngas [5–9], and the highly selective oxidation of light hydrocarbons [10,11]. As OTM materials, perovskite-type oxides (ABO_3) that are mixed ionic and electronic conducting exhibit high oxygen permeability; however, the OTMs reported in the literature have several serious drawbacks, such as chemical instability in reducing conditions, lack of mechanical durability, and deterioration in a CO_2-containing gas atmosphere.

The goal of our project is to develop dense ceramic OTMs that provide oxygen for efficiently and economically producing hydrogen through the reforming of renewable liquid fuels such as ethanol (EtOH) and bio-oil [12]. It has been shown that supplying oxygen with an OTM reduced the cost of methane reforming by ≈30–40% and energy consumption by ≈30% [13]. Supplying oxygen during EtOH reforming increases EtOH conversion and enhances catalyst performance by preventing coke formation [14]. An OTM can supply high-purity oxygen for EtOH reforming by separating it from air without using a separate gas separation unit. Because the OTM is a mixed conductor, the oxygen transport requires neither electrodes nor external power circuitry, i.e., the process is non-galvanic. The oxygen flux through the membrane depends on the membrane's electron and oxygen-ion conductivities, its surface oxygen exchange kinetics, and the oxygen partial pressure (pO_2) gradient across the membrane.

* Corresponding author. Tel.: +1 630 252 3823; fax: +1 630 252 3604.
E-mail address: cpark@anl.gov (C.Y. Park).

0378-7753/$ – see front matter © 2012 Elsevier B.V. All rights reserved.
doi:10.1016/j.jpowsour.2012.04.052

We report here the oxygen permeation properties of the ceramic/metal composites, $Ba_{0.5}Sr_{0.5}Cu_{0.2}Fe_{0.8}O_{3-\delta}$/Ag (BSCF/Ag) as our target OTM materials. In earlier studies, similar cobalt-based perovskite oxides, $La_xSr_{1-x}Co_yFe_{1-y}O_{3-\delta}$ [3] and $Ba_xSr_{1-x}Co_yFe_{1-y}O_{3-\delta}$ [2,4–6,15], were reported to be among the most promising materials in terms of oxygen permeability. The flexible redox behavior of cobalt, however, leads to a large coefficient of thermal expansion and structural instability at intermediate operating temperatures (500–800 °C). Long-term stability, an essential requirement for practical membranes, appears to be better for Co-free BSCF membranes. Efimov et al. found that the oxygen permeation flux of a BSCF membrane maintained a value of ≈ 0.53 mL cm^{-2} min^{-1} for more than 200 h at 750 °C, while the flux through $Ba_{0.5}Sr_{0.5}Co_{0.8}Fe_{0.2}O_{3-\delta}$ (BSCoF) continuously decreased with time [16]. The high electrical conductivity of BSCF, with a maximum reported value of ≈ 45 S cm^{-1} at 620 °C [16], suggests that the BSCF OTM might be useful for intermediate-temperature applications like EtOH reforming.

We initiated our study by the solid-state synthesis of BSCF membranes; however, the samples exhibited structural instability in the form of fine cracks. To improve the structural integrity for the membranes, we fabricated composites that contained 10–40 vol.% Ag. We then sought to determine if our composites were able to produce hydrogen during EtOH reforming. We investigated the structural behavior, the oxygen permeation properties, the microstructure, and hydrogen production during EtOH reforming. We performed EtOH reforming at 600 °C and compared the hydrogen production results with those of an $La_{0.7}Sr_{0.3}Cu_{0.2}Fe_{0.8}O_{3-\delta}$ (LSCF) thin-film tube that were reported previously [17,18].

2. Experimental details

2.1. Membrane preparations

2.1.1. BSCF membrane

$Ba_{0.5}Sr_{0.5}Cu_{0.2}Fe_{0.8}O_{3-\delta}$ (BSCF) powder was prepared by conventional solid-state synthesis. Proper amounts of $BaCO_3$ (Alfa Aesar, 99.997%), $SrCO_3$ (Aldrich, 99.9+%), Fe_2O_3 (Alfa Aesar, 99.99%), and CuO (Johnson Matthey, 99.999%) were ball milled with zirconia media in isopropyl alcohol (IPA) for three days, and then the mixture was dried on a hot plate. The powder mixture was calcined at 850 °C for 10 h in ambient air, and then was milled again overnight. After drying to remove the IPA, the powder was pressed uniaxially into disks (at 5000 psi with a 1-in.-diameter die). Dense ceramic disks were prepared by sintering in air at 950–1000 °C for 10 h.

2.1.2. BSCF/Ag composites

The BSCF disks were found to develop fine cracks after polishing; however, cracks did not develop when BSCF was mixed with Ag powder (Alfa Aesar, 99.9%, 0.7–1.3 μm) in a mortar and pestle to prepare composites with 10–40 vol.% Ag (16.5–54.2 wt.% Ag). The BSCF/Ag powder was ground mildly for more than 30 min with IPA, screened with a 150-μm mesh sieve, and then uniaxially pressed (15,000 lb-force) into a disk (1-in. dia). The sample bars for dilatometry were also prepared in a rectangular die (7.9 × 44.5 mm). Pressed disks and bars were sintered at 920–930 °C for 10 h in ambient air.

2.1.3. Rh catalyst

Rh catalyst was deposited on one face of a BSCF/Ag composite disk to test its effect during ethanol reforming. Rhodium nitrate, $Rh(NO_3)_3 \cdot 2H_2O$ (Alfa Aesar, 99.9%), was dissolved in deionized water, and then XUS binder and BSCF/40 vol.% Ag powder mixture were added to the solution to give a composition of 4 wt.% Rh. Heating the solution with binder and powder at <80 °C while stirring gave a viscous paste that was painted onto the surface of the BSCF/40 vol.% Ag disk. The painted disk was dried in air, installed in the reactor, and heated to 600 °C for an ethanol reforming test.

2.2. Measurements

2.2.1. Dilatometry

The BSCF and BSCF/30-40 vol.% Ag bars (4.54 × 6.78 × 25.00 mm, 2.40 × 6.54 × 24.99 mm, and 2.27 × 6.60 × 25.00 mm, respectively) sintered at 930–950 °C for 10 h in ambient air were measured for dilatometry (Theta Instrument) experiments. The measured temperature was $25 \leq T \leq 830$ °C with a heating and cooling rate of 2 °C min^{-1} in ambient air. The temperature was kept for 2 h at 830 °C. From these measurements, thermal expansion coefficients (TECs) were calculated.

2.2.2. IPA test

Before measuring an OTM's oxygen flux or its hydrogen production during EtOH reforming, the OTM was tested for interconnected porosity and/or microcracks by checking if IPA had penetrated it. Penetration of the OTM by even a small amount of IPA was easily seen as darkening of its surface, and indicated that the OTM contains cracks or interconnected porosity. If IPA did not penetrate an OTM, it was tested on a fixture that allowed separate gases to be flowed over opposite faces of the OTM.

2.2.3. Oxygen permeation measurements

The oxygen permeation flux was measured by sealing polished disks to the end of an Al_2O_3 tube with a spring-loaded assembly [19]. A schematic diagram of the membrane reactor can be found in our previous reports [20–22]. During the measurements, air and ultra-high purity (UHP) He were flowed on the feed and sweep side of the membrane, respectively, at flow rates of 150 mL min^{-1}. The effective membrane's surface area was ≈ 1.27 cm^2. The oxygen concentration in the sweep gas was measured with a Hewlett-Packard 6890 gas chromatograph (GC, Wasson ECE instrumentation). The concentration of nitrogen in the He sweep gas was measured to correct for minor oxygen leakage through the gas seal.

2.2.4. Ethanol reforming

For ethanol reforming tests, silver gaskets were used to make gas-tight seals between the alumina fixture and an Rh catalyst-coated BSCF/40 vol.% Ag disk (thickness = 0.65 mm). After gas-tight seals had formed by heating at 700 °C, the tube was cooled to 600 °C to conduct ethanol reforming tests. The ethanol partial pressure (p_{EtOH}) was fixed on the Rh-coated side of the disk by bubbling UHP He or N_2 through absolute ethanol at 23 °C, giving $p_{EtOH} \approx 0.067$ atm, while air was flowed on the other side of the disk. Both gases flowed at a rate of 200 mL min^{-1} during the measurements. The total flow rate for the EtOH side was 200 mL min^{-1}, but the flow rate of carrier gas through the EtOH bath was only 100 mL min^{-1}, giving 7.21 mL min^{-1} of $EtOH_{In}$. The other 100 mL min^{-1} of carrier gas flowed without EtOH, an arrangement that allowed us to continuously flow gas to the EtOH side when we switched the carrier gas. The concentrations of products from ethanol reforming were measured by GC. After the ethanol reforming test, the Rh-coated disk's microstructure was examined with a JEOL 5400 scanning electron microscope (SEM).

3. Results and discussion

3.1. Characteristics of BSCF and BSCF/Ag

Fig. 1a and b show secondary electron images of a BSCF disk sintered at 1000 °C for 10 h in ambient air. The cross-sectional

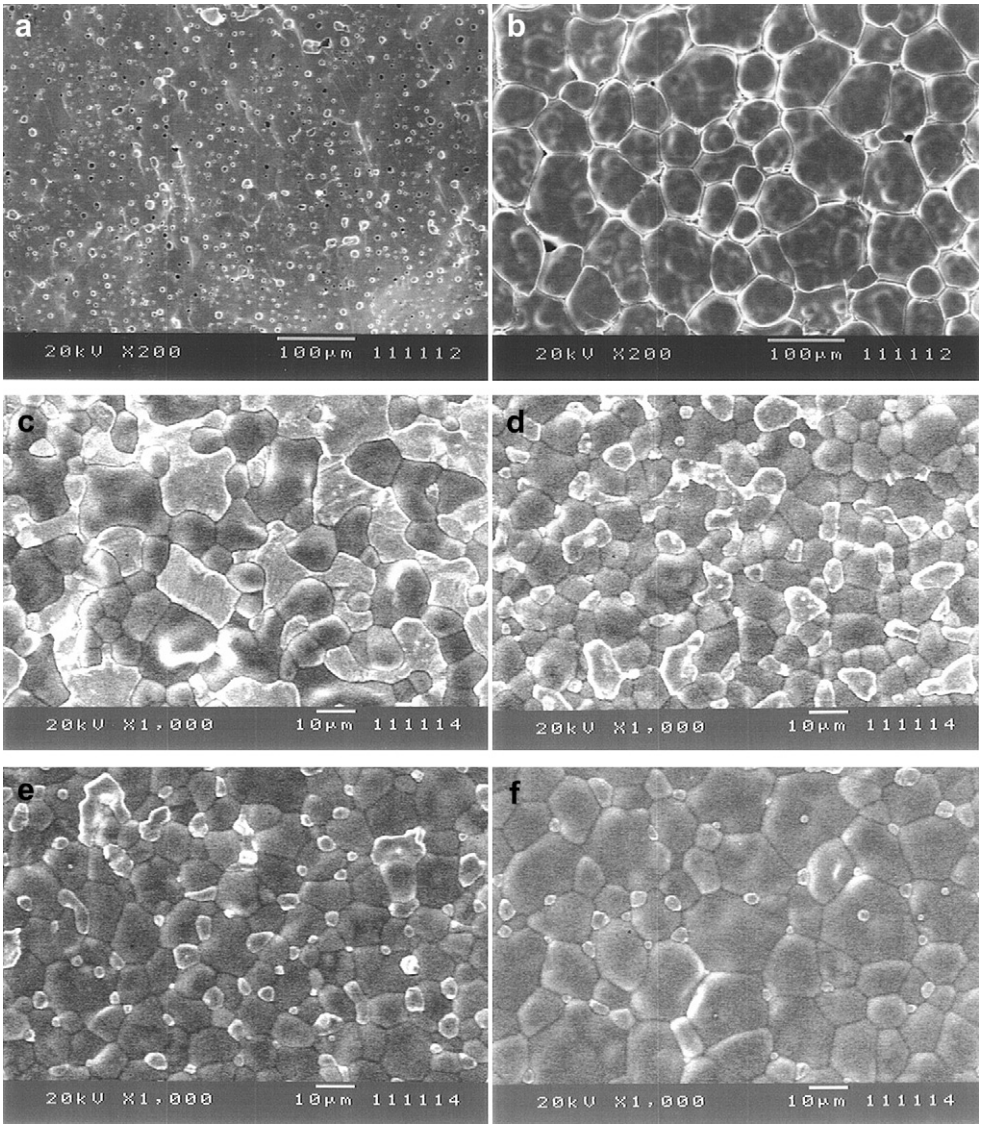

Fig. 1. Secondary electron images of BSCF and BSCF/Ag disks: (a) BSCF – cross sectional fracture, (b) BSCF – surface, (c) BSCF/40 vol.% Ag – surface, (d) BSCF/30 vol.% Ag – surface, (e) BSCF/20 vol.% Ag – surface, and (f) BSCF/10 vol.% Ag – surface of the sample.

fracture in Fig. 1a includes small isolated pores, and Fig. 1b represents the surface microstructure of the sample. No secondary phase was found from the analysis using energy-dispersive X-ray spectroscopy (EDS, Thermo scientific), and the grain size was in the range of 40–130 μm. Although the BSCF disk looks apparently dense and IPA had not penetrated through the sample, several line cracks appeared on the surface after the disk was polished.

To eliminate the line cracks inside the sample and to enhance the mechanical strength, we made BSCF/Ag composite disks. Fig. 1c through 1f shows the microstructure of the composite's surface. The highest silver content was 40 vol.% (Fig. 1c), and the silver phase was placed mainly on the grain boundary of the BSCF. No pores were seen on the surface, and the systematic changes of the Ag phase are evident by its contrast with the ceramic phase. The sintering temperature of the composites was 920–930 °C for 10 h, which was lower than that used for pure BSCF (950–1000 °C for 10 h). The grain sizes of the BSCF phase in the BSCF/Ag composites were ≤25 μm, and the grains look to have packed well. The BSCF/Ag composites appeared to be crack-free and exhibited improved mechanical properties as the Ag content increased.

The crystal structure the BSCF and BSCF/Ag disks was investigated by powder X-ray diffraction (XRD, Philips X-Pert 8856 X-ray diffractometer) using Cu Kα radiation. As shown in Fig. 2, the XRD pattern of the BSCF disk (top) was completely indexed with a cubic unit cell having lattice parameter $a = 3.962(0)$ Å. The cell parameter reported for BSCF fabricated by a sol–gel method is $a = 3.9434(4)$ Å [16]. The small difference in the cell parameter is attributed to the differences in synthesis method and/or sintering temperature. The XRD powder pattern of the BSCF/40 vol.% Ag was also well indexed, and the peaks were separated from the Ag phase.

The thermal expansions of the BSCF, BSCF/30 vol.% Ag, and BSCF/40 vol.% Ag composites were measured in the temperature range $25 \leq T \leq 830$ °C in air. The measurements were made over thermal cycles at heating and cooling rates of 2 °C min^{-1}. Rectangular composite bars sintered at 930–950 °C for 10 h in air were used for dilatometry measurement (Theta Dilatometry). Fig. 3 shows the thermal expansion results for the BFCF, BSCF/30 vol.% Ag, and BSCF/40 vol.% Ag bars. Based on the dilatometry data, the thermal expansion coefficients (TECs) were calculated and are summarized

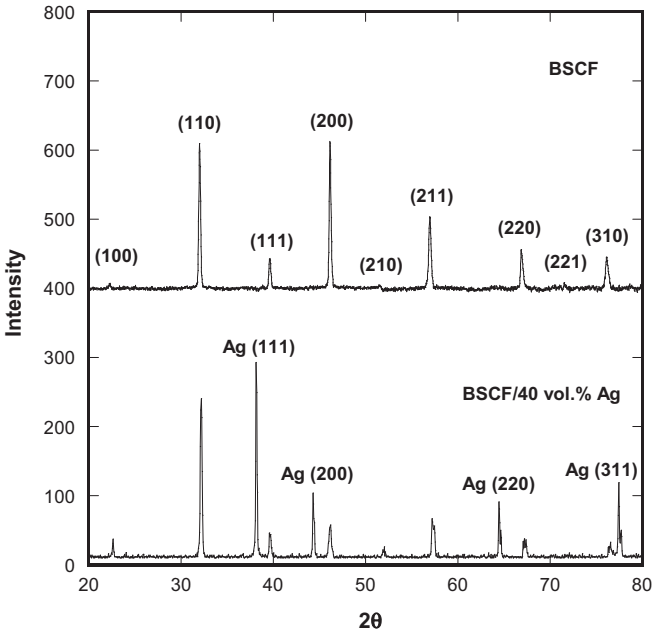

Fig. 2. XRD patterns for BSCF (top) and BSCF/40 vol.% Ag (bottom) disks.

in Table 1. The TECs of the BSCF/40 vol.% Ag composite were $\sim 18.2 \times 10^{-6}$ K^{-1} and $\sim 22.3 \times 10^{-6}$ K^{-1} at $100 \leq T \leq 500$ °C and $500 \leq T \leq 830$ °C, respectively. There were no big differences in the TECs of the composites; however, the average TEC values for the composites were slightly higher than those reported for BSCF [16] without Ag at lower temperature ≤500 °C, while the composites gave slightly lower TECs at higher temperature ≥500 °C. For comparison, we measured the TECs of BSCF, which showed reasonably close to that of the reference [16]. The sample's expansion and contraction (with heating and cooling) are quite reproducible except for minor differences at $500 \leq T \leq 750$ °C that may be due to the kinetics of oxygen insertion and removal from the lattice.

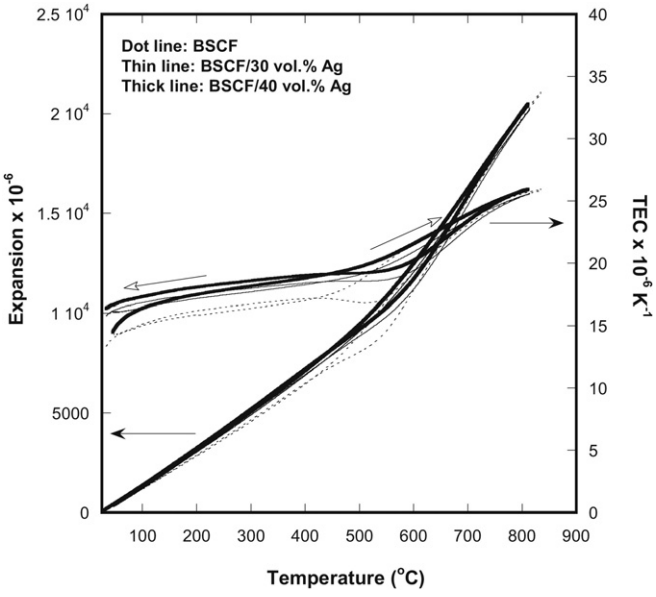

Fig. 3. Thermal expansion data for BSCF, BSCF/30 vol.% Ag and BSCF/40 vol.% Ag bars. The open arrows indicate the direction of the temperature profile.

Table 1
Thermal expansion coefficients of BSCF and BSCF/Ag composites.

OTM	TEC[a] × 10^{-6} K^{-1}		Source
	100 ~ 500 °C	500 ~ 830 °C	
BSCF	16	23	[16]
BSCF	15.2 ~ 16.8 (16.5)	16.8 ~ 25.8 (21.5)	This work
BSCF/30 vol.% Ag	16.4 ~ 19.1 (17.7)	19.1 ~ 25.6 (21.8)	This work
BSCF/40 vol.% Ag	16.4 ~ 19.6 (18.2)	19.6 ~ 26.0 (22.3)	This work

[a] The values in parentheses are the average TECs.

3.2. Oxygen permeability

Based on promising results in the literature [16], we tried to measure the oxygen flux of BSCF disks, but were unable because the disks developed fine cracks after sintering. Since the BSCF/Ag composites with 10–40 vol.% Ag did not develop cracks, we measured their oxygen flux as a function of temperature. Because the composite mechanical properties appear to improve with the Ag content, we focused on composites with ≥30 vol.% Ag, even though composites with <30 vol.% Ag give a slightly higher oxygen flux due to their higher volume fractions of the OTM. While the addition of Ag is not practical on a large scale, it allowed us to use BSCF for the purpose of our experiment.

Fig. 4 shows the temperature dependence of the oxygen permeation flux for BSCF/10–40 vol.% Ag composites. The solid line indicates the oxygen flux for an LSCF thin-film disk (≈14 μm) for comparison. The figure inset gives the thickness of each OTM and the Ag content for the BSCF/Ag composites. For all samples, N_2 leakage was measured to be ≤0.13% on the sweep side at 830 °C while UHP He (150 mL min^{-1}) and air (150 mL min^{-1}) flowed on the sweep and the feed side, respectively. This means that the measured sweep gas (He) contained less than 0.13% (<0.2 mL min^{-1}) of N_2. After correcting for leakage, the oxygen transfer rate of the BSCF/Ag disk (0.33-mm-thick at 830 °C) to the sweep gas was 1.10 mL min^{-1}. Without the correction for leakage,

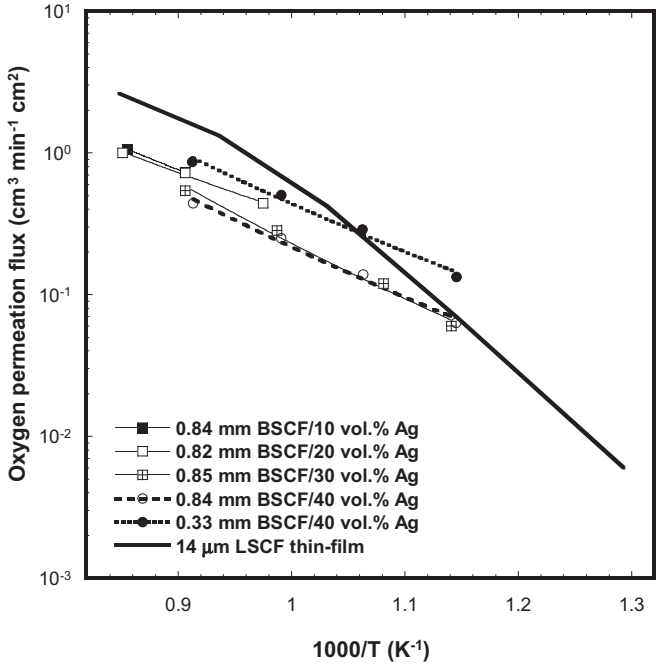

Fig. 4. Temperature dependence of the oxygen permeation flux of BSCF/10–40 vol.% Ag composites. The solid line indicates oxygen permeation flux of the reference, $La_{0.7}Sr_{0.3}Cu_{0.2}Fe_{0.8}O_{3-\delta}$ (LSCF) thin film [19].

an oxygen transfer rate of 1.14 mL min^{-1} would have been calculated, indicating that >96% of oxygen transported through the membrane (not from the leak). After checking the leakage, we measured the oxygen permeation fluxes of the composites with decreasing temperature. The oxygen permeation fluxes of the BSCF/Ag composites were lower than those of an LSCF thin-film disk at high temperatures, but a slightly thinner (0.33 mm) BSCF/40 vol.% Ag composite gave a higher flux below ~650 °C. No major difference in the oxygen flux was found for the composites with 30 and 40 vol.% Ag over the whole temperature range. Moreover, the oxygen flux of the disks (thickness = 0.84–0.85 mm) was similar to that for a much thinner LSCF thin-film disk (thickness = 14 μm) at 600 °C, indicating that higher oxygen flux values should be achievable with BSCF/Ag thin disks or films. As expected, a BSCF/40 vol.% Ag disk polished down to ≈0.33 mm achieves more than two times higher oxygen flux than that of a ≈0.84 mm-thick disk at 600 °C. The apparent activation energies (E_a) for the BSCF/Ag composites were calculated from the slopes of the data in Fig. 4 and found to be in the range of 0.52–0.81 eV, lower than the values of E_a = 1.15–1.35 eV reported for LSCF [19].

The addition of Ag also markedly improved the sample durability during the measurements. For the BSCF/10–20 vol.% Ag samples, nitrogen leakage developed as the temperature decreased from 900 °C (at 830 °C for 10 vol.% Ag and at 750 °C for 20 vol.% Ag); however, N_2 leakage did not develop for BSCF/30–40 vol.% Ag samples down to 600 °C. The results suggest that the Ag content in BSCF/Ag composites should be ≥30 vol.% in order for the composites to be useful for applications at temperatures below ≤700 °C.

3.3. Ethanol reforming

Ethanol reforming tests were done with a BSCF/Ag disk, an LSCF thin-film tube, and a dense, oxygen-impermeable Al_2O_3 tube as a "blank". The BSCF/Ag disk contained 40 vol.% Ag, had thickness, 0.65 mm and geometric surface area of 1.27 cm^2, and was coated with porous Rh catalyst. The LSCF tube contained a dense LSCF thin-film (thickness ≈30 μm) on the outside of a porous LSCF tube (≈40 vol.% porosity) with O.D. of 0.96 cm, I.D. of 0.67 cm, and length of 5.1 cm. The geometric surface area of the LSCF thin-film was 15.3 cm^2. The LSCF tube was used without any catalyst. The blank tube had an I.D. of 0.63 cm and length of 5.1 cm. Table 2 summarizes the results from reforming tests at 600 °C, and Fig. 5 shows the products that were formed. A trace of C_2H_6 was also detected during the tests but is not shown in Fig. 5.

The residence time during the test with the LSCF tube was calculated by subtracting the volume of the substrate and that of the feed inlet tube from the volume inside the OTM film, giving a reaction volume of 1.94 cm^3 and a residence time of 16 sec for a feed flow rate of 7.21 mL min^{-1}. Defining the reaction volume in this way, the reactants were within ≈0.5 cm of the OTM film on the tube's outer surface. If the reaction volume is defined similarly for the test with the disk, i.e., the reaction volume extended 0.5 cm from the OTM's surface, the reaction volume for the disk (0.61 cm^3) is smaller due to its smaller surface area, and the residence time (5 sec) is also smaller. The residence time during the test with the blank was 8 sec.

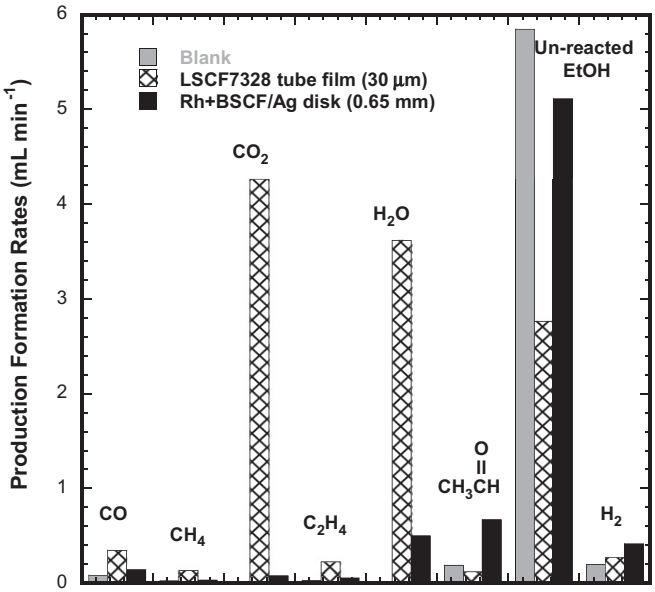

Fig. 5. Flow rates of species in product stream during EtOH reforming at 600 °C with an oxygen-impermeable Al_2O_3 blank tube, an LSCF thin-film tube, and a BSCF/40 vol.% Ag disk.

Fig. 5 compares the compositions of the product streams during EtOH reforming at 600 °C with the three types of sample. Whereas the formation rates of CO, H_2O, and CO_2 were negligible with the blank, they all increased significantly when the blank was replaced by the LSCF tube. The flow rate of un-reacted EtOH in the product stream decreased by >50% (from 5.8 to 2.8 mL min^{-1}) with the LSCF tube, giving an EtOH conversion of ≈62% versus ≈19% with the blank. Although not large, the hydrogen formation rate was also slightly higher with the LSCF tube than with the blank. These results clearly indicate that the LSCF tube increased the ethanol conversion, but the high H_2O formation rate indicates that much of the hydrogen produced by reforming was consumed by reaction with oxygen.

The ethanol conversion with the BSCF/Ag disk was low (≈29%) but was higher than conversion with the blank (19%) even though the residence time was longer with the blank. The higher conversion for the disk despite a shorter residence time suggests that the increase in EtOH conversion was caused by the catalyst, the oxygen supplied by the OTM, or a combination of the oxygen and catalyst. The major products of reforming with the disk were hydrogen, water, and acetaldehyde (CH_3CHO), suggesting that dehydrogenation of ethanol (Eq. 1) is the dominant reaction. Although the water production rate is much smaller with the disk than with the tube, the formation of water with the disk indicates that the hydrogen production rate is lower than the acetaldehyde production rate because some hydrogen reacts to form water. Acetaldehyde can subsequently decompose via Eq. 2, but the low production rates of

Table 2
Results of EtOH reforming experiments at 600 °C.

OTM	Ethanol reforming at 600 °C				
	OTM Thickness	H_2 (mL min^{-1})	H_2O (mL min^{-1})	Carbon balance (%)	EtOH conversion (%)
Blank tube	–	0.196	~0	84.6	19.2
LSCF Thin-film tube	~30 μm	0.274	3.62	75.8	61.8
BSCF/40 vol.% Ag disk + Rh catalyst	0.65 mm	0.418	0.50	82.5	29.4

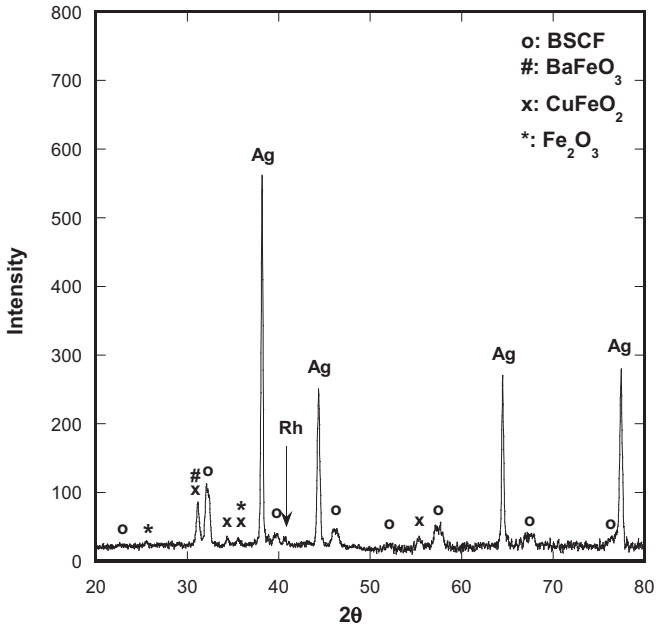

Fig. 6. XRD pattern of an Rh catalyst-coated BSCF/40 vol.% Ag disk after ethanol reforming experiment.

CO and CH_4 suggest that this reaction is not prevalent with the disk, although it is perhaps more prevalent with the tube.

$$C_2H_5OH \rightarrow CH_3CHO + H_2 \quad (1)$$

$$CH_3CHO \rightarrow CO + CH_4 \quad (2)$$

Ethanol can also decompose to ethylene and water through dehydration (Eq. 3), but the low ethylene formation rate (Fig. 5) for both the tube and the disk indicates that this is not a favorable reaction.

$$C_2H_5OH \rightarrow C_2H_4 + H_2O \quad (3)$$

The much lower flow rate of un-reacted EtOH and significantly larger production rates of CO_2 and H_2O (Fig. 5) indicate that EtOH conversion was much higher with the tube than with the disk. Using the oxygen flux data (Fig. 4) and geometric surface areas of the membranes, the amount of transported oxygen at 600 °C is estimated to be ≈6 times higher for the tube than for the disk. As was found in comparing EtOH reforming rates with an OTM and a blank, the injection of oxygen by the OTM seems to have enhanced the EtOH conversion, although the longer residence time with the tube also contributed to the higher conversion.

The carbon balance and conversion of ethanol during EtOH reforming were defined as follows:

$$\text{Carbon balance} = \frac{\text{Carbon}_{\text{Out}}}{\text{Carbon}_{\text{In}}} \times 100 = \frac{CO + CH_4 + CO_2 + 2C_2H_4 + 2C_2H_6 + 2CH_3CHO + 2EtOH}{2EtOH} \times 100 \quad (4)$$

$$\text{EtOH conversion} = \frac{\text{EtOH}_{\text{In}} - \text{EtOH}_{\text{Out}}}{\text{EtOH}_{\text{In}}} \times 100 \quad (5)$$

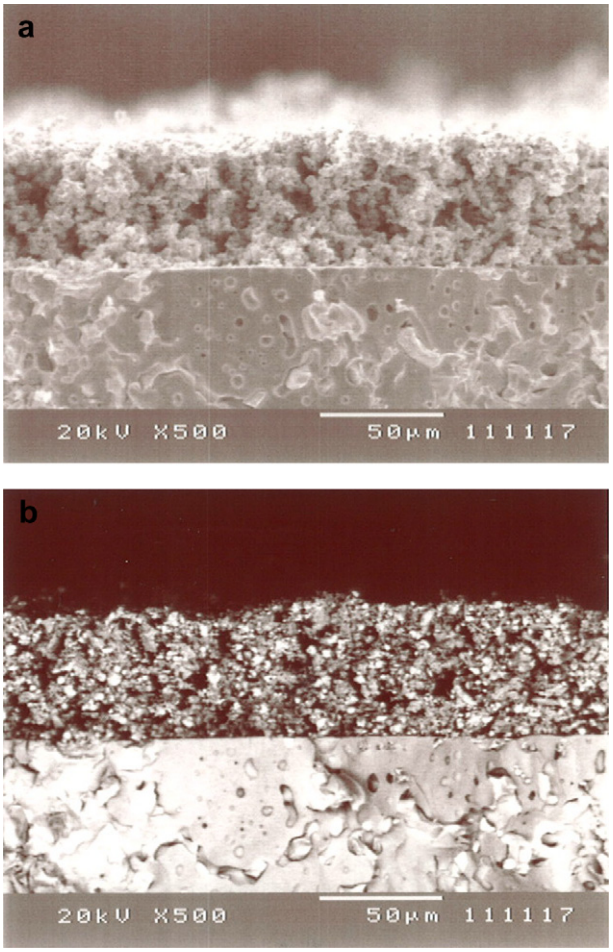

Fig. 7. (a) Secondary and (b) backscatter electron images of an Rh catalyst-coated BSCF/40 vol.% Ag disk after ethanol reforming experiment.

where the $\text{Carbon}_{\text{In/Out}}$ and $\text{EtOH}_{\text{In/Out}}$ were calculated with units of mol min^{-1}. The disk's ethanol conversion rate was lower than the tube's (29% vs. 62%), because the disk had a much smaller active area (≈1.27 cm^2 vs. ≈15.3 cm^2) and was much thicker (0.65 mm vs. 30 µm). Despite its lower EtOH conversion and its smaller active area, the total hydrogen production rate (HPR) of BSCF/40 vol.% Ag was 0.42 mL min^{-1}, which is 56% higher than that of the LSCF tube. The carbon balance during the tests was in the range 76–85%. Only small amounts of coke were found after the reforming experiments, but were probably sufficient to explain the low carbon balance.

Fig. 6 shows the XRD powder pattern of the BSCF/40 vol.% Ag disk coated with catalyst that was used in the ethanol reforming test. The BSCF perovskite peaks including silver and rhodium were relatively well preserved and several decomposed products were also detected. The main decomposed product is believed to be $BaFeO_3$, and small amounts of the $CuFeO_2$ and Fe_2O_3 phase are also

identified. Fig. 7a and b show the secondary and backscatter electron images for the cross-sectional fracture surface, respectively. Isolated porosity is evident in the BSCF/40 vol.% Ag membrane, seen at the bottom of the images. The porous catalyst-containing layer on top of the BSCF/40 vol.% Ag disk had a thickness of ≈ 50 μm. The EDS analysis confirmed the presence of Rh catalyst. The bright particles in the backscattered electron image (Fig. 7b) are either Ag or Rh particles.

4. Conclusions

The results demonstrate that a dense OTM can enhance the reforming of renewable liquids. We fabricated cobalt-free oxygen transport membranes, namely, BSCF/Ag composites, and evaluated their oxygen permeation fluxes. Based on the data of oxygen permeation flux, an Rh catalyst-coated BSCF/40 vol.% Ag composite was tested for producing hydrogen from ethanol reforming at 600 °C. The BSCF/Ag composite was found to increase the hydrogen production from ethanol reforming by supplying high-purity oxygen from air. The Rh catalyst increased the selectivity for hydrogen and decreased coke formation in the reactor. The crystal structure, microstructure, and EDS analysis of the BSCF/Ag composite were investigated before and after the EtOH reforming experiment. Further study should be done to evaluate the chemical stability of OTMs, the effects of EtOH concentration, gas flow rates, and OTM thickness during EtOH reforming at lower temperatures (≈ 500 °C). The effects of the Rh-catalyst (or other catalysts) on reforming with tubular OTM with larger active area (≈ 15 cm^2) should be studied.

Acknowledgments

Work supported by the U.S. Department of Energy (DOE), Energy Efficiency and Renewable Energy, Fuel Cell Technologies Program, under Contract DE-AC02-06CH11357.

References

[1] C.S. Chen, S. Ran, W. Liu, P.H. Yang, D.K. Peng, H.J.M. Bouwmeester, Angew. Chem. Int. Ed. 40 (4) (2001) 784–786.
[2] H.H. Wang, Y. Cong, W.S. Yang, J. Membr. Sci. 210 (2002) 259–271.
[3] Y. Teraoka, H.M. Zhang, S. Furukawa, N. Yamazoe, Chem. Lett. 14 (1985) 1743–1746.
[4] A.C.V. Veen, M. Rebeilleau, D. Farrusseng, C. Mirodatos, Chem. Commun. 1 (2003) 32–33.
[5] H.H. Wang, Y. Cong, W.S. Yang, Catal. Today 82 (2003) 157–166.
[6] C.S. Chen, S.J. Feng, S. Ran, D.C. Zhu, W. Liu, H.J.M. Bouwmeester, Angew. Chem. 115 (2003) 5354–5356.
[7] C.Y. Tsai, A.G. Dixon, W.R. Moser, Y.H. Ma, AIChE J. 43 (11A) (1997) 2741–2750.
[8] P.N. Dyer, R.E. Richards, S.L. Russek, D.M. Taylor, Solid State Ionics 134 (2000) 21–33.
[9] U. Balachandran, J.T. Dusek, P.S. Maiya, B. Ma, R.L. Mieville, M.S. Kleefisch, C.A. Udovich, Catal. Today 36 (1997) 265–272.
[10] H.H. Wang, Y. Cong, W.S. Yang, Chem. Commun. 14 (2002) 1468–1469.
[11] F.T. Akin, Y.S. Lin, Catal. Lett. 78 (1–4) (2002) 239–242.
[12] G. Rabenstein, V. Hacker, J. Power Sources 185 (2008) 1293–1304.
[13] U. Balachandran, C.Y. Park, T.H. Lee, Y. Lu, J.J. Picciolo, J.E. Emerson, S.E. Dorris, Distributed reforming of renewable liquids using oxygen transport membranes, DOE Hydrogen and Fuel Cell Program, FY, Argonne National Laboratory, 2010, Annual Progress Report.
[14] F. Frusteri, S. Freni, V. Chiodo, S. Donato, G. Bonura, S. Cavallaro, Int. J. Hydrogen Energy 31 (2006) 2193–2199.
[15] Z. Shao, W. Yang, Y. Cong, H. Dong, J. Tong, G. Xiong, J. Memb. Sci. 172 (2000) 177–188.
[16] K. Efimov, T. Halfer, A. Kuhn, P. Heitjans, J. Caro, A. Feldhoff, Chem Mater. 22 (2010) 1540–1544.
[17] C.Y. Park, T.H. Lee, S.E. Dorris, U. Balachandran, Int. J. Hydrogen Energy 35 (2010) 4103–4110.
[18] U. Balachandran, C.Y. Park, T.H. Lee, Y. Lu, J.J. Picciolo, J.E. Emerson, S.E. Dorris, Distributed reforming of renewable liquids using oxygen transport membranes, DOE Hydrogen and Fuel Cell Program, FY, Argonne National Laboratory, 2011, Annual Progress Report.
[19] C.Y. Park, T.H. Lee, S.E. Dorris, Y. Lu, U. Balachandran, Int. J. Hydrogen Energy 36 (2011) 9345–9354.
[20] S.-J. Song, T.H. Lee, E.D. Wachsman, L. Chen, S.E. Dorris, U. Balachandran, J. Electrochem. Soc. 152 (11) (2005) J125–J129.
[21] T.H. Lee, S.E. Dorris, U. Balachandran, Solid State Ionics 176 (2005) 1479–1484.
[22] C. Zuo, T.H. Lee, S.-J. Song, L. Chen, S.E. Dorris, U. Balachandran, M. Liu, Electrochem. Solid State Lett. 8 (12) (2005) J35–J37.